

7.2 OBSERVATIONS AND NUMERICAL MODELLING OF MOUNTAIN WAVES OVER THE ORGAN AND SAN ANDRES MOUNTAINS OF NEW MEXICO

P.A. Haines*
U. S. Army Research Laboratory
White Sands Missile Range, NM 88002

D. J. Grove
U. S. Army Research Laboratory
Aberdeen Proving Grounds,, MD 21005-5067

W.-Y. Sun
Purdue University
West Lafayette, IN 47907-2051

W. -R Hsu
National Taiwan University
Taipei, Taiwan

B. T. MacCall
U. S. Army Research Laboratory
White Sands Missile Range, NM 88002

INTRODUCTION

White Sands Missile Range (WSMR) lies mainly in the lee of the Organ and San Andres Mountains in south central New Mexico. Together, the two mountain ranges form a nearly unbroken, 150 km long, south to north oriented barrier that rises 1 to 1.5 km above the surrounding terrain. This barrier is both quite steep and generally quite narrow, ranging from a maximum width of 20 km to 5 km. During late winter and much of the spring, there is often strong westerly flow aloft over the southwestern U.S. Frequently, strong inversions at heights somewhat above that of the highest terrain complicate the flow's response as it traverses the steep barrier. Consequently, WSMR experiences many mountain and lee wind events in this part of the year. Because of the variations in elevation, it is possible during a given situation at WSMR to have both sub- and super-critical flows in juxtaposition, greatly complicating the resulting flow and presenting significant challenges to numerical forecasting models.

Many U.S. Army missions are significantly impacted by the highly variable weather conditions in and around complex terrain such as at WSMR, but the Army's capability to forecast and diagnose such conditions remains limited. To better understand and to evaluate and improve the capability of high resolution numerical models to forecast the effects of terrain on weather conditions, the U.S. Army Research Laboratory (ARL) collected surface data from five 10 m instrumented towers sited in the lee of the Organ Mountains during the first 3 months of

2004. In addition, data were collected from the White Sands Missile Range (WSMR) Surface Automated Meteorological System (SAMS) and other nearby surface stations such as the Remote Automated Weather Stations (RAWS) and the wind profiling radar at WSMR. The total data set enables meso- β and meso- γ scale depiction of the wind flow in the lee of the Organ mountains; this is augmented in the vertical using horizontal and vertical wind components from the NOAA Profiling Network wind profiling radar located at WSMR. The total data set enables meso- β (2 to 20 km) and - γ (200 m to 2 km) scale depiction of the wind flow in the lee of the Organ Mountains; this is augmented in the vertical direction using horizontal and vertical wind component data from the WSMR wind profiling radar.

The following sections provide a brief description of the numerical forecasting model employed, comparisons of the numerical results with the observations, details of the model's scalability characteristics, and a discussion of the potential for future applications.

2. NUMERICAL FORECASTING MODEL

The NTU/Purdue nonhydrostatic numerical model, hereafter referred to as the NTU/P model, has been under development over the last 8 years to predict atmospheric motions and conditions for both the mesoscale (200 m to 200 km) and large scale turbulence (20 to 200 m) scales. The model explicitly

solves the fully compressible nonhydrostatic system of equations (Hsu and Sun, 2001) and builds on the proven success of a preceding hydrostatic numerical model (Chern, 1994, Sun et al. 1991, Sun and Chern, 1993, Haines et al., 1997). The vertical coordinate of the model is defined as:

$$\sigma = \frac{p_0(z) - p_0(z_{top})}{p_0(z_{surface}) - p_0(z_{top})}, \quad (1)$$

where p_0 , the reference atmosphere pressure, is strictly a function of height. Although this vertical coordinate appears to be the usual σ -pressure coordinate used in many hydrostatic models, the pressure in (1) is not a function of time, so the position of each grid point is fixed in time. Hence, the model employs, strictly speaking, a σ - z coordinate. The advection terms are calculated with the Sun (1993) advection scheme. The diffusion process is parameterized through a level 2.5 turbulence scheme.

The use of the prognostic density equation avoids the need to solve the full diabatic pressure equation, which is instead diagnosed through the equation of state for a perfect gas,

$$p = \rho R T, \quad (2)$$

where T is temperature, and R is the gas constant. Equivalent potential temperature, θ_e is used as the prognostic variable in the heat equation, where θ_e is defined as:

$$\theta_e = \theta + \left(\frac{\theta}{T}\right) \frac{L_v}{c_p} q_v, \quad (3)$$

and θ is potential temperature, c_p is the specific heat at constant pressure, q_v is the specific humidity of water vapor, and L_v is the latent heat of vaporization. The total specific humidity, $q_w = q_v + q_l$ (where q_l is the liquid water content) is also a semi-conservative quantity in the absence of precipitation.

The fully explicit solution system employed by the NTU/P model is simple, memory-efficient, and is accurate for high frequency waves. Thus, it can provide a good comparison basis for the implementation of semi-implicit or other more time-efficient schemes to ensure their accuracy. As with many forecasting models, the Arakawa-C grid is employed in the horizontal, with density and vertical velocity staggered with respect to each other in the vertical direction. The model uses a two-tier forward-backward solution procedure that is neutral in time with respect to both sound waves and internal gravity waves. This forward-backward scheme for sound and gravity waves means that the new solution values corresponding to the current time immediately replace those of the preceding time during the calculation so that only one storage array is required. Therefore,

this scheme uses only half of the memory space required by centered finite difference schemes typically employed in numerical forecasting models. In addition, this scheme produces no computational modes (i.e., numerical noise), thus avoiding the need for a time filter. The compressible set of equations admits fast sound waves necessitating a small time step for their solution. The consequences of the small time step are mitigated through the use of a time-splitting technique (Gadd, 1978) in which the time integration is split into multiple stages; the corresponding time steps depend on the physical time scales of the calculated terms which involve advection, sound and other fast waves, and diffusion. The details of the numerical scheme are presented in Hsu and Sun (2001). The NTU/P model software package has been fully parallelized using the Message Passing Interface (MPI) library.

3. OBSERVATION DETAILS

From January into March 2004 the ARL set up five instrumented towers (10 m in height) in the lee of the Organ Mountains. Each tower measured and recorded the wind direction and wind speed at a height of 10 m above ground level, as well as pressure, humidity, and temperature at a height of 2 m above the ground. The pressure instruments used were inter-compared, yielding an accuracy of +/- 10 pascals or better. Meanwhile, ARL also collected data from several of the nearby WSMR SAMS and RAWS sites to provide a fairly detailed picture of the surface air flow in and around the Organ Mountains. During the 3-month observation period, there were several down-slope wind storms and a variety of blocked-flow episodes. Besides the collected surface data, we obtained the vertical and horizontal wind profiles recorded by the two collocated wind profiling radars at White Sands that are situated about 15 to 20 km downwind of the mountains. These radar systems provide data coverage from about 500 m above their ground elevation (4000 feet) to about 17 km above sea level.

4. SIMULATION RESULTS

4.1 Lee Waves / Hydraulic Jump

On 25 January 2004, a down-slope wind storm occurred along the lee of the Organ and San Andres Mountains; it included the formation of a train of lee waves which extended downwind across the Tularosa Basin and a hydraulic jump just to the lee of the mountains that was well-observed by the ARL and SAMS pressure sensors. These storms occur occasionally at WSMR, but this day's storm was especially noteworthy because the surface and other observations were able to document many of its facets, thus enabling detailed comparisons with the numerical model results.

To simulate this case, the NTU/P model's three-dimensional (3D) grid was set up with a vertical spacing of 300 m and a horizontal resolution of 1 km. Digital Terrain Elevation Data (DTED) level 1 terrain data was used to generate (via bi-linear interpolation) a 201 x 201 grid (with 1 km spacing) for a 200 km x 200 km region centered just to the east of the San Augustine Pass. Initially, when the NTU/P model's terrain smoothing algorithm was employed to eliminate two-delta x variations and to smooth the terrain at the periphery of the model domain, we found that the maximum terrain heights were somewhat less than the actual terrain. By experimenting, we found that a two step process could result in maximum terrain heights quite close to the actual values. In the first step, each initial terrain height above 1400 m was increased by an amount equal to 40 percent of the difference between the initial terrain height and 1400 m. Then, in the second step, the resulting combination of adjusted and unadjusted terrain heights was smoothed. Of course, it was not possible to obtain the maximum height of very narrow features such as the Organ Mountains ridge, but as shown in Fig. 1 the maximum height of the Organ Mountains (2720 m) and of the southern massif of the San Andres Mountains (2189 m) are well replicated in the terrain field used in this study. At the same time, the horizontal breadths of the mountains and the height of the Tularosa basin are preserved and agree extremely well with the real terrain.

Figure 2 reveals the details of the El Paso, TX sounding at 12Z (1200 UCT) on 25 January 2004. Note the strong inversion at about 600 hPa or about 4000 m above sea level (asl). Calculated values of the Scorer Parameter (Scorer, 1949)

$$l^2 = \frac{N^2}{U^2} - \frac{1}{U} \frac{d^2U}{dz^2} \quad (4)$$

are shown in this figure for the areas below and above the inversion. Here, U is the horizontal velocity (m/s), and N is the Brunt-Väisälä frequency (1/s).

It is known that a significant decrease of the Scorer Parameter in the vertical when gravity waves are likely should result in lee waves downstream from the terrain. The model and observations all strongly support the occurrence of lee waves.

Using the sounding shown in Fig. 2, along with the assumptions of a no-slip surface and no Coriolis force, the NTU/P model was initialized and integrated for 3 hours. The simulation results are presented in Figs. 3 through 6. Figure 3 compares the model-predicted wind field with the recorded observations at 0800 hrs local time (1500 UCT) on 25 January 2004. In this figure, the NTU/P model's surface wind field is represented by the wind vectors, which indicate a strong down-slope flow on the lee side of the Organ and San Andres Mountains. In a band oriented

mainly south-to-north just east of the mountains, the model's surface winds abruptly lessen and then either reverse (from W to E) or remain considerably diminished; this hydraulic jump corresponds to the strong adverse pressure gradient shown by the pressure perturbations.

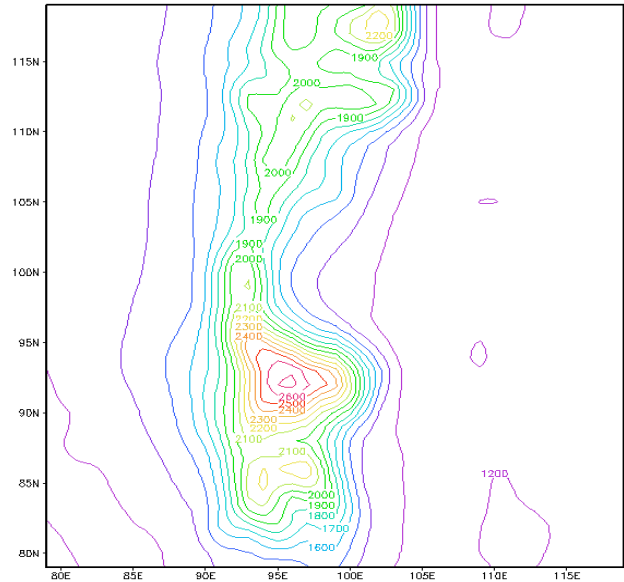


Fig. 1: NTU/P model domain terrain field for the central part (i:80-120; j:80-120) of the 201x201 grid; terrain heights are in meters above sea level and contours are every 100 m.

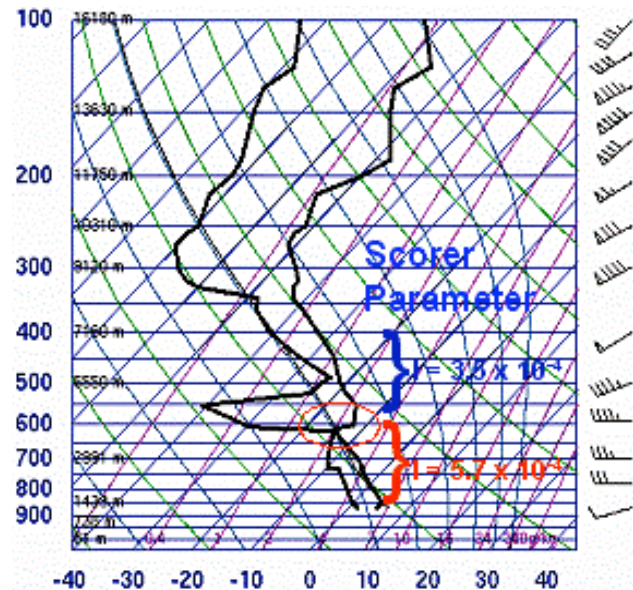


Fig. 2: El Paso, TX sounding for 25 January 2004 at 12Z.

The transitions to reversed flow appear to the northeast of the higher terrain areas such as the Organ Mountains and the higher terrain to the north of

the WSMR post. The reversed regions are about 5 km wide; to the east of the reversed region, the model surface winds return to westerly but are not as strong as in the strong down-slope flow area just to the lee of the Organ Mountains. Still farther to the east, about 20 to 25 km east of the mountain chain, there is another diminished or reversed wind region which is not as continuous or strong as that immediately to the lee of the mountains.

The observed winds are shown by the yellow arrows in Fig. 3. The model's wind field agrees quite closely with the actual wind field, except that the observed winds at the San Augustine Pass are stronger than the model's prediction. This pass is approximately 1 to 2 km wide. While the model's grid spacing is 1 km, its effective resolution is no better than 5 km. Hence, we expect that a numerical model will require a grid spacing of about 300 to 400 m or less to adequately resolve the wind flow at the San Augustine Pass.

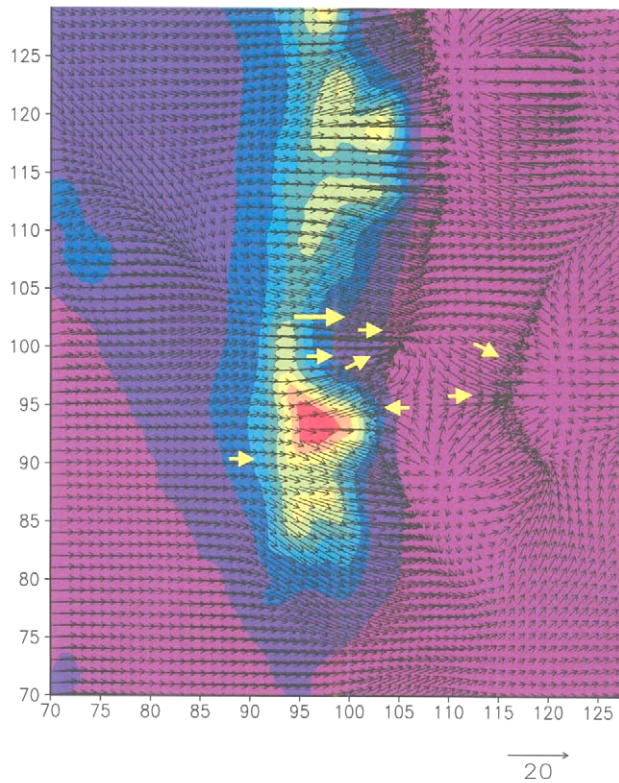


Fig. 3: Predicted surface wind field from the NTU/P model simulation of the January 25 down-slope wind storm case at WSMR (after 3 hours of model integration); yellow arrows indicate the observed wind field.

Figure 4 compares the model's predicted surface nonhydrostatic pressure perturbations with the observed pressure perturbations from the ARL and SAMS pressure sensors. The colored contour lines show the NTU/P model's 3 hour forecast of the surface pressure perturbations; the values range

(approximately) from 0 to -200 pascals (-2 hPa). There is a band of maximum negative perturbation pressure running south-to-north along the lee side of the Organ Mountains. A little farther east, the model shows a band of little or no perturbation pressure. Even farther east, there is another band of negative perturbation pressure. These model-predicted bands continue across the Tularosa basin in connection with the lee waves.

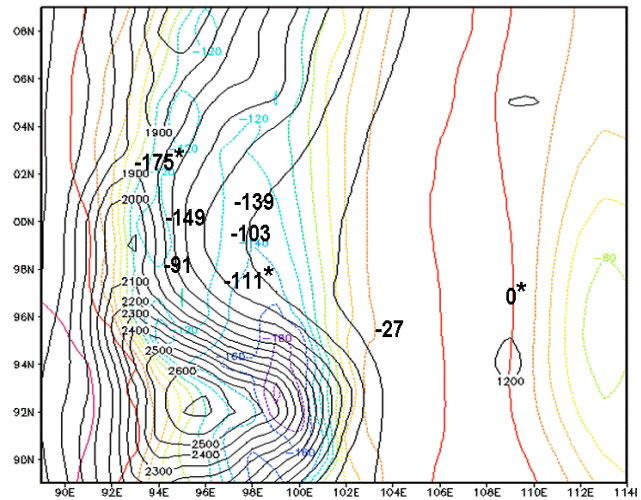


Fig. 4: Predicted surface pressure perturbations (color contours, in pascals) from the NTU/P model simulation of the 25 January down-slope wind storm case at WSMR; bold numbers (in black) indicate the observed pressure perturbations from the ARL and SAMS observations.

The observations shown in Fig. 4 include the ARL instrumented towers and the SAMS sites (indicated by *) in this area. The observed pressure perturbations were very carefully extracted through pressure reduction to a common datum plane at 1295 m. With the exception of the observation at the San Augustine Pass, the height of this plane minimized the vertical distance over which pressure reduction was done for the observations, consequently minimizing the error of the extracted pressure perturbations.

Except for the San Augustine site, the model's predicted wind field and pressure perturbation bands are in good agreement with the observations. In addition, the model's predicted pressure perturbation compares well with the observation from the Oro Grande gate SAMS which is located far to the east of the area shown in Fig. 4.

Vertical cross-sections of vertical and horizontal wind components and the pressure perturbations support the occurrence of a hydraulic jump in conjunction with the wind reversal and adverse pressure gradient shown in Figs. 3 and 4. Fig. 5 shows a west to east cross section of the NTU/P

model's predicted vertical velocity field for 0800 hrs local time (1500 UCT) on 25 January 2004 located north of the WSMR post, approximately intersecting the San Augustine Pass and, more importantly, coinciding with the location of the White Sands wind profiling radar (shown by the dark vertical line in Fig. 5). The model prediction shows partially trapped lee waves extending eastward across the Tularosa Basin. The maximum vertical velocities are greater than 3 m/s. Using the Scorer Parameters calculated from the El Paso sounding, the theoretical wavelength of 13 to 14 km compares fairly closely to the model-predicted wavelength of around 14 to 15 km. The observed lee waves, which are well represented by the model's surface winds, are in fairly good agreement with the wind profiler observations, and are consistent with a decrease (with height) in the Scorer Parameter.

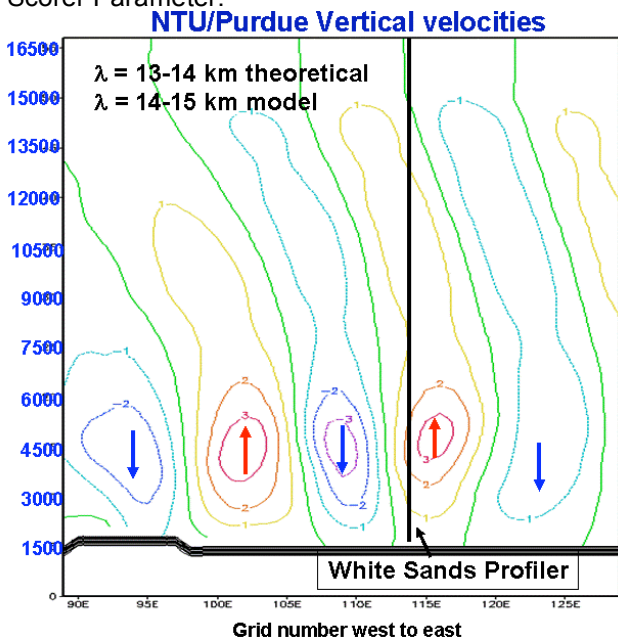


Fig. 5: NTU/P model-predicted vertical velocity field (m/s) at 0800 hrs local time on 25 January 2004 along a west to east cross-section that intersects with the location of the WSMR (vertical black line) wind profiling radar.

Fig. 6 compares the NTU/P model's predicted vertical velocities with the WSMR wind profiler data on 25 January during approximately the same time interval (0700 to 0900 hrs). In this figure, the y-axis represents the height (m) asl, while the x-axis is the vertical velocity (m/s). The model's vertical velocity profiles are shown by continuous color lines; the corresponding times are shown in the legend on the upper right hand side of this figure. The model shows two peaks in vertical velocity: one maximum at about 4500 m and the second at about 12000 m. The model predicted a steady drop in the lower peak's

vertical velocities from 0730 to 0830 hrs, with essentially no change between 0830 and 0900 hrs, while the upper peak's vertical velocities were steadier over this same time period.

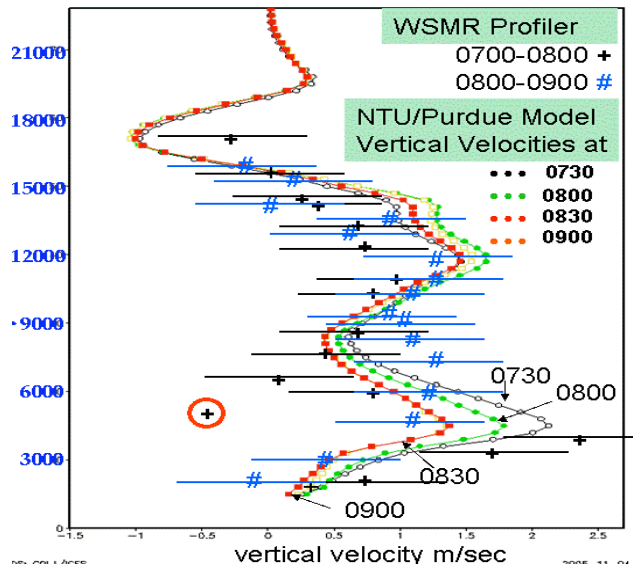


Fig. 6: Comparison of the NTU/P model-predicted vertical velocity profiles with the observed velocity profiles at the WSMR wind profiling radar location on 25 January 2004.

In Fig. 6, the vertical velocity profiles recorded by the WSMR wind profiler are shown by the black pluses and blue pound signs. These are the mean values, respectively, for the "0700-0800" and "0800-0900" time periods. What is shown has been smoothed by using a running 5 point mean value, because the individual point values are quite noisy. The wind profiler is believed to have an accuracy of +/- 0.5 m/s, so the corresponding error bars were included for each observed value. The observations show that the lower maximum's vertical velocities decrease going from hour 1 to 2 but the upper maximum's vertical velocities are roughly the same. It should be mentioned that the profiler's winds are obtained from processing of radial components along three beams that are not quite vertically oriented so the obtained value is probably more representative of the vertical velocity over a volume of space rather than being a point measurement. Despite these limitations, the NTU/P model's predictions of vertical velocity are in general agreement with the observations at the WSMR profiler site.

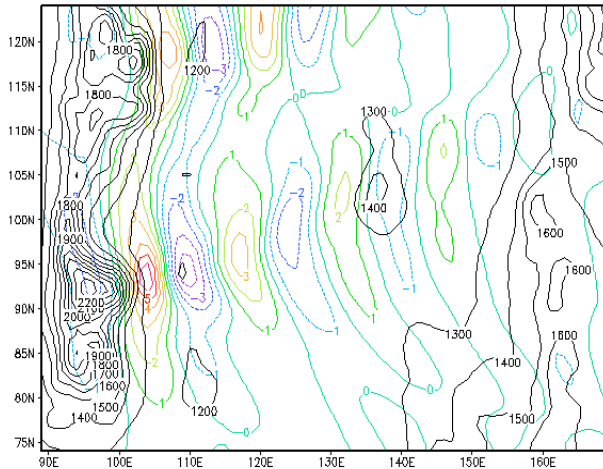
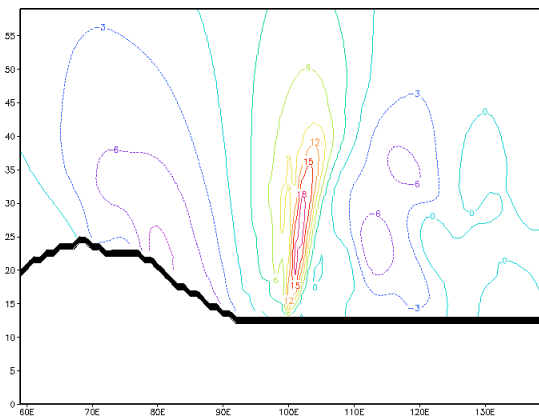


Fig. 7: Horizontal cross-section showing the NTU-P vertical velocities for 0800 25 January 2004. The figure extends across the Tularosa Basin and shows at least 4 full lee waves in an ENE direction from the Organ Mountains.

Fig 7 shows the NTU-P vertical velocity field at about 6000 m asl for 0800 25 January 25, 2004. The lee waves extend across the Tularosa Basin and appear to be propagating in an ENE direction in the direction of the mean wind. Another similar train of lee waves can be seen at the top of the figure associated with the San Andres Mountains just to the north of the Organ Mountains.

Some higher resolution simulations have been done for the vicinity of the Organ Mountains. These show more detail on the lee wave/ hydraulic jump just downwind from the Organs.

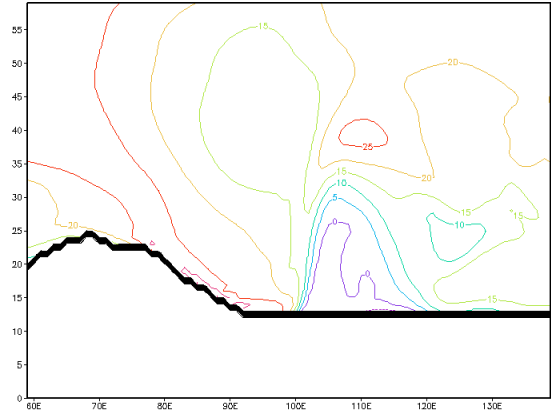


©ADS: COLA/RES

Fig. 8: Vertical cross-section through the Organ Mountains showing the NTU-P vertical velocities for 0800 25 January 2004.

Fig. 8 shows a vertical cross-section of the NTU-P vertical velocity field for a west to east cross-section

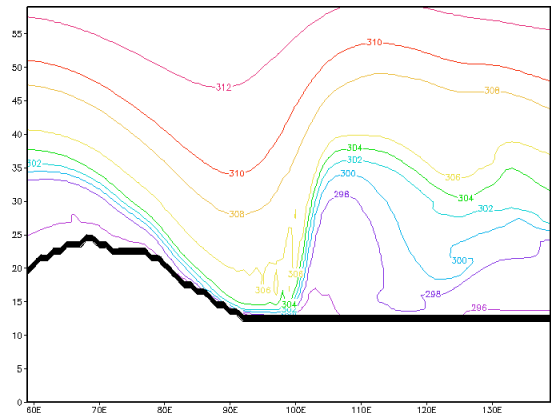
that runs through the Organ Mountains. At the higher resolution, higher vertical velocities, up to 15 m sec⁻¹ can be seen. The strongest vertical velocities are also more narrowly located confined than was seen in the coarser resolution simulations.



©ADS: COLA/RES

Fig. 9: Vertical cross-section through the Organ Mountains showing the NTU-P u-component horizontal velocities for 0800 25 January 2004

Fig 9 shows a vertical cross-section of the NTU-P u-component horizontal velocity field for a west to east cross-section that runs through the Organ Mountains. Note the flow reversal in conjunction with the strong vertical velocities shown above.



©ADS: COLA/RES

Fig. 10: Vertical cross-section through the Organ Mountains showing the NTU-P θ_v for 0800 25 January 2004

Fig 10 shows a vertical cross-section through the Organ Mountains of the NTU-P θ_v at 0800 on 25 January 2004

4.2 Blocking Effects / Down-Slope Winds

The blocking effects of mountains on air flow have been studied for years. However, most studies have been conducted with either an idealized mountain or for synoptic-mesoscale systems due to the difficulties of collecting very high resolution data or even developing a reliable forecasting model. Also, until recently, computational limitations have prevented the numerical solution of this high-resolution, 3D problem in a reasonable amount of time. The results from this study indicate that the high resolution NTU/P model is capable of reproducing the details of the flow in very pronounced terrain under different prevailing wind conditions. Using the same grid and terrain data as in the preceding case, the model was initialized with the El Paso, TX sounding at 12Z on 19 January 2004 (see Fig. 11) and integrated for 3 hours.

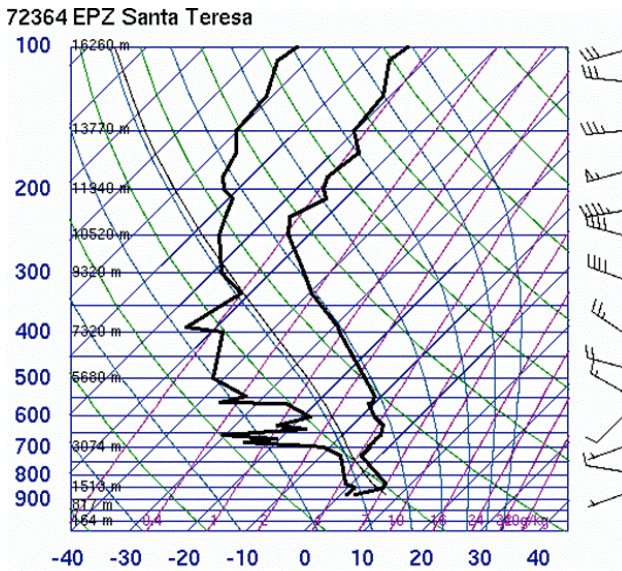


Fig. 11: El Paso, TX sounding for 19 January 2004 at 12Z.

Because of the variation in terrain heights, some of the areas to the lee of the Organ Mountains on 19 January are subject to blocking, while the flow for other areas is supercritical and down-slope winds develop. The model-predicted overall flow situation is quite complex, as indicated by Fig. 12. The model-predicted wind field is represented by the colored vectors. There is low level blocked flow (BF) in the lee of the Organ Mountains, but also down-slope wind (DW) flow on the south side of the Organs and to the north of the WSMR post.

The Froude Number (defined in the upper right hand corner of Fig. 12) provides a good measure of whether air will go over or around a terrain obstacle. Because of the different height scales, in this case, the Froude Number is less than 1 for flow trying to go

directly over the Organ Mountains but is greater than 1 elsewhere so it can go over the terrain. Hence, we have a juxtaposition of sub- and super-critical flow, which helps produce the complexities shown. Note that the observations generally confirm the model predictions, although the observed winds at the San Augustine Pass are stronger than those given by the model.

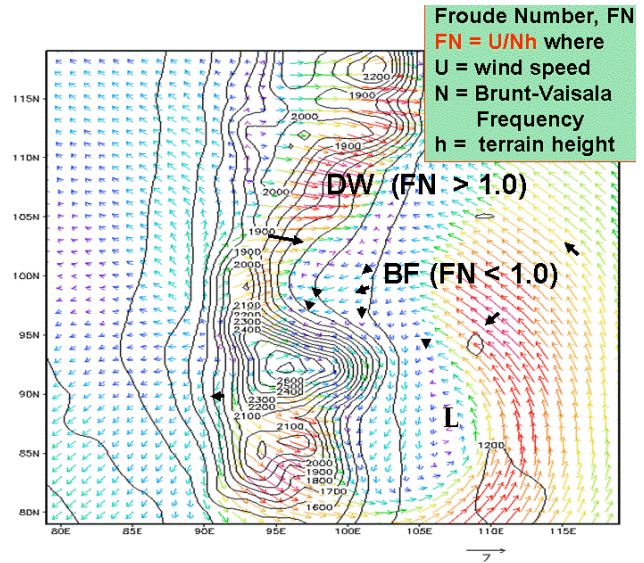


Figure 12: Predicted surface wind field (color vectors) from the NTU/P model simulation for 19 January 2004 at WSMR (after 3 hours of model integration); black arrows indicate actual observations (10 m above the ground).

The blocking effects of the WSMR terrain, particularly in the lee of the Organ Mountains, have been shown in SAMS and other data Grove and Haines (2002). Grove and Haines noted that the wind flow shown by the SAMS stations was consistent with the formation of a lee vortex. However, the number of SAMS stations near the Organ Mountains is limited, and additional measurements would be required to fully reveal the actual flow. The kinds of blocking predicted by the NTU/P model has also been seen in the observational results for westerly and southwesterly flow cases in which the Froude Number was less than 0.5. During the January to March 2004 observations, fully and partially blocked flow, as well as lee waves and hydraulic jumps in the lee of mountains, were recorded.

5. SCALABILITY RESULTS

As indicated in Section 2, the NTU/P model software package has been fully parallelized using Message Passing Interface (MPI) library routines. To evaluate the scalability characteristics of this advanced forecasting model, we ran the case described in Subsection 4.1 (down-slope wind storm case at WSMR on January 25, 2004) on the

unclassified 1024-node Linux Network Evolocity II cluster at the ARL Major Shared Resource Center. Maintaining a fixed problem size of four million grid points (200x200x100), we varied the number of processors from 4 to 128 and ran the test case for three hours of simulation time. Table 1 shows the total wall clock times, speed-up factors (relative to the 4-processor case), and percentages of optimum speed-up achieved for the various numbers of processors. As the table indicates, the NTU/P model scales very well on the ARL MSRC's Linux cluster.

Table 1. Scalability Results for NTU/P Model

Number of Processors	Wall Clock Time (s)	Actual Speed-up Factor	Optimum Speed-up Factor	% of Optimum Speed-up
4	78523	reference	--	--
8	40287	1.95	2	97.5
16	20925	3.75	4	93.8
32	11114	7.07	8	88.3
64	5998	13.09	16	81.8
128	3658	21.47	32	67.1

6. CONCLUSIONS

The NTU/P model was applied to several well-observed real terrain cases for the Organ and San Andres Mountains in southern New Mexico. On 25 January 2004, a down-slope wind storm in the lee of these mountains was accompanied by a hydraulic jump and lee waves, all of which were well-observed. The NTU/P model was initialized with the 12Z El Paso sounding for 25 January and run for several hours. As shown, the model successfully predicted much of the atmospheric phenomena observed on that day. The model was also applied to partially and fully blocked flow conditions on the WSMR terrain. With a Froude Number of less than 0.5, the model shows that the terrain causes pronounced blocking, along with the formation of a lee vortex. The model-predicted surface wind fields are consistent with the local WSMR surface flows observed for these kinds of conditions. On 19 January 2004, the WSMR surface observations showed super- and sub-critical flows. The NTU/P model was initialized with the 12Z El Paso sounding for January 19 and run for several hours. The model's predicted wind flow agrees fairly well with the intricacies of the complex flow that were actually observed.

Knowing the surface and boundary layer wind fields benefits the Army in several important ways.

The characterization of dispersion and diffusion of various biological/chemical agents in the battlefield requires detailed information including wind speed, wind direction, and the variability of both, all of which can be reliably provided by high resolution numerical modeling. Also, some munitions are significantly affected by the low-level wind field as they maneuver in acquiring and engaging their target; obtaining a reliable forecast of the target area wind field will allow them to be more optimally aimed. In addition, the low-level wind and turbulence fields are linked; hence, knowing where to avoid severe turbulence and adverse winds will greatly benefit Army aviation missions, especially those involving helicopters, unmanned aerial vehicles, and para-drop operations. Finally, the wind environment and embedded turbulence significantly affect acoustic propagation, so accurate numerical forecasts of wind and turbulence fields will help acoustic detection and avoidance programs.

While the results presented in this paper demonstrate the feasibility of producing high resolution forecasts of complex wind flow caused by and occurring in proximity to mountainous terrain, much additional work remains to be done. The NTU/P model used here was found to have high scalability characteristics, so that with the model domain used in this paper, it is possible to obtain the forecast results over 21 times faster using 128 processors versus use of only 4. This means that a three hour forecast can be completed in about an hour. If a semi-implicit approach is implemented to solve the vertical momentum equation, and higher computational efficiency is attained, it should be possible to more than halve the NTU/P model's run time. The ARL MSRC will soon be installing a new Linux Network Advanced Technology Cluster with 1122 quad-core compute nodes. This significant increase in computing power will enable us to generate more detailed weather forecasts using even higher resolution grids (e.g., 100-m grid point spacing, with billions of grid points) for regions with complex terrain. This will help us determine the levels of detail and accuracy that can be achieved using the currently available (state-of-the-art) numerical weather forecasting models. While increased grid resolution (i.e., smaller grid spacing) may lead to more accurate forecasts, it may also reveal model deficiencies that can be corrected, or at least improved. As computing power continues to increase, we anticipate that a practical numerical weather forecasting tool will eventually be developed for use in the field. The ultimate goal of this work is to provide Army commanders with accurate assessments of meteorological conditions in the battlefield (in near real-time) to assist in their strategic planning and decisions.

ACKNOWLEDGEMENTS

This work was supported in part by a grant of computer time from the DoD High Performance Computing Modernization Program (HPCMP) at the ARL MSRC, Aberdeen Proving Ground, MD.

REFERENCES

- Chern, J. D., 1994: Numerical simulations of cyclogenesis over the western United States, Ph. D. Thesis, Department of Earth and Atmospheric Sciences, Purdue University, 178 pp.
- Gadd, A. J., 1978: A split explicit integration scheme for numerical weather prediction. *Quart. J. Roy. Met. Soc.*, 104, 569-582.
- Grove, D. J., and P. A. Haines, 2002: Fine scale numerical prediction of atmospheric flow in complex terrain. 2002 DRI Report, US Army Research Laboratory, Adelphi, MD.
- Haines, P. A., J. D. Chern. and W. Y. Sun, 1997: Numerical simulation of the Valentine's Day storm during WISP 1990. *Tellus*, 49A, 595-612.
- Hsu, W. R., and W. Y. Sun, 2001: A time-split, forward-backward numerical model for solving a nonhydrostatic and compressible system of equations. *Tellus*, 53A, 279-299.
- Scorer, R. S., 1949: Theory of waves in the lee of mountains. *Quart. J. Roy. Meteor. Soc.*, 75, 41-56.
- Sun, W. Y., 1993: Numerical experiments for advection equation. *J. of Comput. Phys.*, 108, 264-271.
- Sun, W. Y., and J. D. Chern, 1993: Diurnal variation of lee-vortexes in Taiwan and surrounding area. *J. Atmos. Sci.* 50, 3404-3430.